nature climate change

Article

https://doi.org/10.1038/s41558-023-01757-7

Asymmetric influence of forest cover gain and loss on land surface temperature

Received: 27 September 2022

Accepted: 4 July 2023

Published online: 3 August 2023

Check for updates

Yongxian Su[1,2], Chaoqun Zhang[1,2], Philippe Ciais[3], Zhenzhong Zeng[4], Alessandro Cescatti[5], Jiali Shang[6], Jing Ming Chen[7], Jane Liu[7], Ying-Ping Wang[8], Wenping Yuan[2], Shushi Peng[9], Xuhui Lee[10], Zaichun Zhu[11,12], Lei Fan[13], Xiaoping Liu[2], Liyang Liu[1,2,3], Raffaele Lafortezza[14,15], Yan Li[16], Jiashun Ren[1,2], Xueqin Yang[1,2] & Xiuzhi Chen[2] ✉

The direct biophysical effects of fine-scale tree cover changes on temperature are not well understood. Here, we show how land surface temperature responds to subgrid gross tree cover changes. We find that in many forests, the biophysical cooling induced by enhanced evapotranspiration due to tree cover gain is greater in magnitude than the warming from tree cover loss. Therefore, the goal of no biophysical warming effects from tree cover changes could be achieved by regaining a fraction of previously lost tree cover areas. This percentage differs between different forest biomes, ranging from 75% in tropical to 83% in temperate forests. Neglecting this asymmetric temperature effect of fine-scale tree cover change ignores the fact that biophysical feedbacks continue to cause surface temperature changes even under net-zero tree cover changes. Thus, it is necessary to account for gross, rather than net, tree cover changes when quantifying the biophysical effects of forests.

Forests store 45% of terrestrial carbon and remove from the atmosphere a large amount of carbon dioxide released by human activities to mitigate global warming[1,2]. This process leads to a global biogeochemical cooling effect by reducing the radiative forcing of carbon dioxide[3]. In addition, forests influence the land–atmosphere exchange of energy and water[4–9] and exert direct biophysical effects on global surface temperatures through radiative processes (albedo)[10] and non-radiative processes (latent and sensible heat fluxes)[11–13]. Forests also have indirect biophysical feedbacks on climate through atmospheric coupling, for example, atmospheric circulation, cloud formation and precipitation[4,14]. During the twenty-first century, there have been dramatic changes (land cover conversions and tree cover changes in forests

[1]Guangdong Provincial Key Laboratory of Remote Sensing and Geographical Information System, Guangdong Open Laboratory of Geospatial Information Technology and Application, Guangzhou Institute of Geography, Guangdong Academy of Sciences, Guangzhou, China. [2]Guangdong Province Data Center of Terrestrial and Marine Ecosystems Carbon Cycle, Guangdong Province Key Laboratory for Climate Change and Natural Disaster Studies, School of Ecology, School of Atmospheric Sciences, School of Geography and Planning, Sun Yat-sen University, Guangzhou, China. [3]Laboratoire des Sciences du Climat et de l'Environnement, IPSL, CEA-CNRS-UVSQ, Université Paris-Saclay, Gif sur Yvette, France. [4]School of Environmental Science and Engineering, Southern University of Science and Technology, Shenzhen, China. [5]European Commission, Joint Research Centre, Ispra, Italy. [6]Ottawa Research and Development Centre, Agriculture and Agri-Food Canada, Ottawa, Ontario, Canada. [7]Department of Geography and Planning, University of Toronto, Toronto, Ontario, Canada. [8]CSIRO Environment, Clayton South, Victoria, Australia. [9]College of Urban and Environmental Sciences, Peking University, Beijing, China. [10]School of the Environment, Yale University, New Haven, CT, USA. [11]School of Urban Planning and Design, Shenzhen Graduate School, Peking University, Shenzhen, China. [12]Key Laboratory of Earth Surface System and Human-Earth Relations, Ministry of Natural Resources of China, Shenzhen Graduate School, Peking University, Shenzhen, China. [13]School of Geographical Sciences, Southwest University, Chongqing, China. [14]Department of Soil, Plant and Food Sciences, University of Bari "Aldo Moro", Bari, Italy. [15]Beijing Forestry University, Beijing, China. [16]State Key Laboratory of Earth Surface Processes and Resources Ecology, Beijing Normal University, Beijing, China. ✉e-mail: chenxzh73@mail.sysu.edu.cn

 https://doi.org/10.1038/s41558-023-01757-7

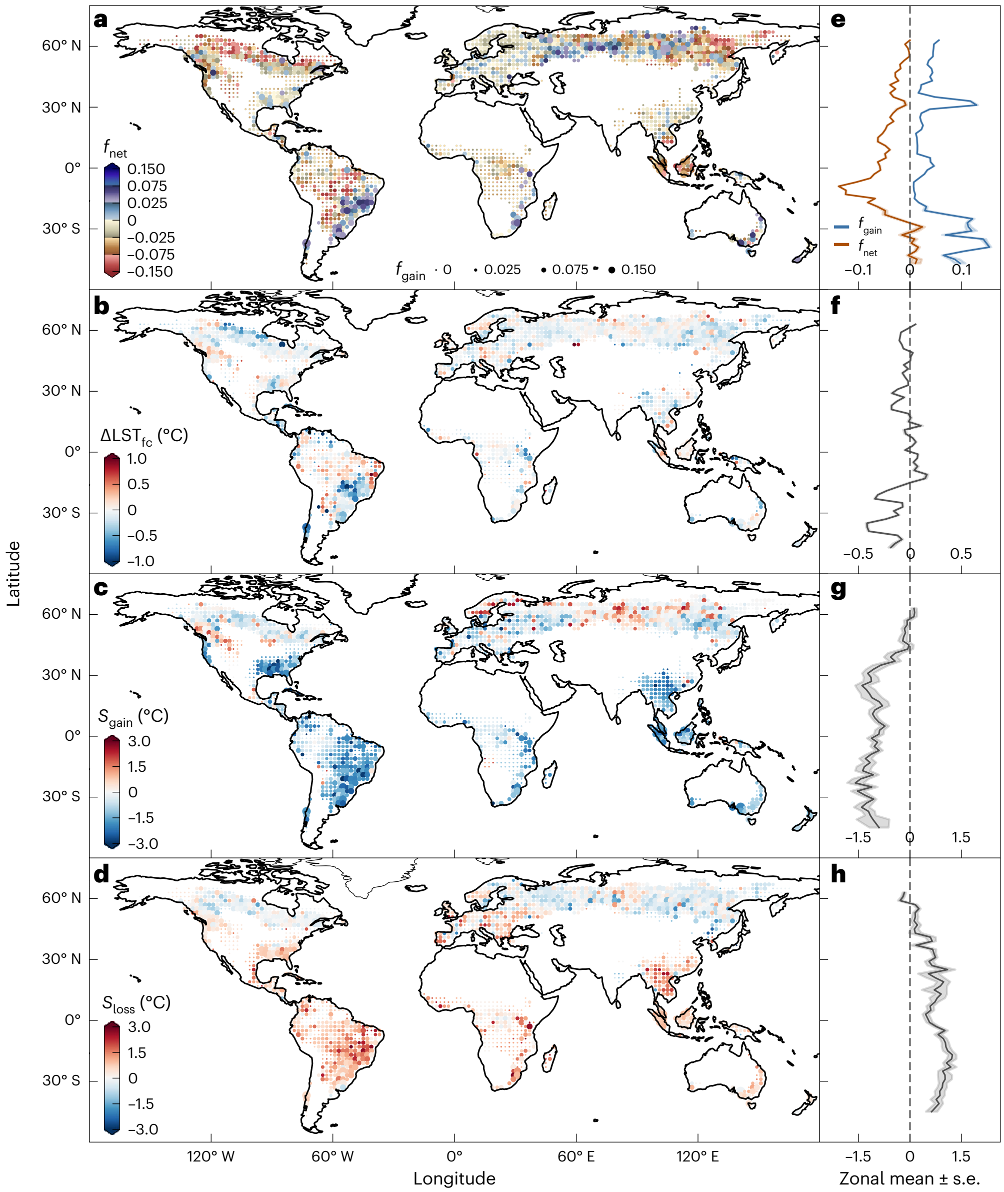

Fig. 1 | Global tree cover changes and their direct biophysical effects on daily mean LST. a, Net fractional change in tree cover (f_{net}) over 0.05° disturbed grid cells that remained forests from 2000 to 2012. **b**, The biophysical effects of tree cover gains and losses on daily mean land surface temperature (ΔLST_{fc}) in disturbed forests. **c**, Sensitivity (S_{gain}) of the daily mean ΔLST_{fc} to gross tree cover gain (f_{gain}). **d**, Sensitivity (S_{loss}) of the daily mean ΔLST_{fc} to gross tree cover loss (f_{loss}). The dots in **a**–**d** are spaced at 2° for both latitude and longitude. **e**–**h**, Zonal mean values of changes in tree cover fractions (**e**), ΔLST_{fc} (**f**), S_{gain} (**g**) and S_{loss} (**h**) averaged into 2° latitude bins, respectively. Shading represents 1 s.e.

remaining forests) in global forests[15,16], affecting their biogeochemical trace gas exchanges[11] and biophysical processes[5,9,17–19].

At the global scale, studies on the biogeochemical[11,20,21] and biophysical temperature effects[22–24] of forests have mainly focused on land cover change such as afforestation and deforestation. The biogeochemical effect is quantified by calculating the carbon difference between forest and neighbouring non-forest grid cells, which is then converted to a global temperature change. The biophysical effect is quantified by interpreting spatial differences in temperature, mainly satellite-based land surface temperature (LST)[21]. These approaches rely on space-for-time analogies where spatial gradients in carbon storage or LST between forest and neighbouring non-forest are used as proxies for estimating temporal changes of biogeochemical or biophysical effects[7,25].

However, fine-scale tree cover changes (gains and losses) have occurred in forests remaining forests worldwide[15], mainly due to natural disturbance, forest management practices and other changes in canopy density[26,27]. While such tree cover gains and losses in established forests are not a land cover conversion, they can still impact the global carbon balance[28,29]. High-resolution satellite carbon data have been used to assess such biogeochemical implications induced by fine-scale tree cover changes based on the space-for-time analogy method[11,20,21]. Nevertheless, challenges remain for quantifying the direct biophysical LST effects induced by fine-scale tree cover changes[5,18,30–36]. This research question is crucial because, currently, LST can only be monitored globally from satellites with frequent revisits at 1 km resolution, whereas changes in tree cover can be assessed at a finer scale of 30 m. Others developed a time-series analysis method to estimate LST change caused by direct biophysical effects of 30 m resolution net tree cover changes using satellite-based data[5,37]. This approach was, however, only applied to net changes in tree cover[5,30] and did not investigate

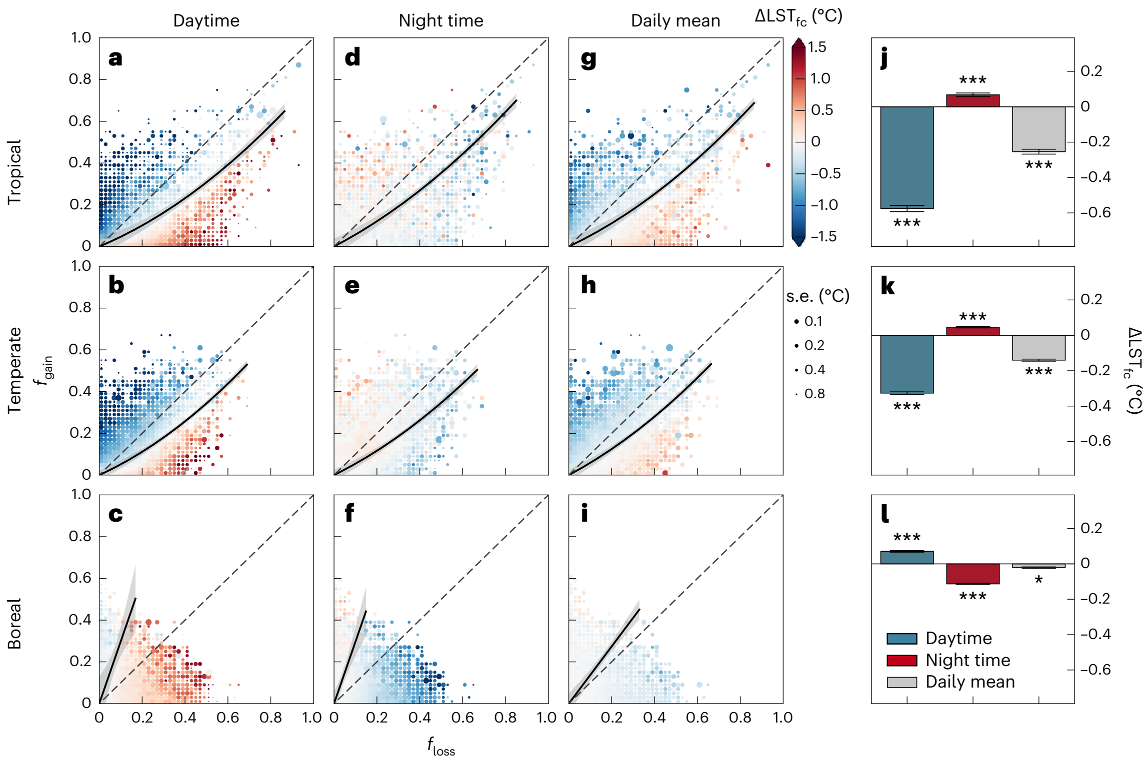

Fig. 2 | Asymmetric biophysical effects of tree cover gain and loss on LST. **a**–**i**, The biophysical effects of various fractions of tree cover gain (f_{gain}) and loss (f_{loss}) on daytime (**a**–**c**), night time (**d**–**f**) and daily mean (**g**–**i**) land surface temperature (ΔLST_{fc}). **a**,**d**,**g**, tropical; **b**,**e**,**h**, temperate; **c**,**f**,**i**, boreal. Each cell in the bubble matrix shows the mean ΔLST_{fc} observed for a given combination of f_{gain} and f_{loss} within 0.05° grid cells from 2000 to 2012 reported on the *x* and *y* axes in the 0.02 bin, respectively. Red denotes a warming effect ($\Delta LST_{fc} > 0.02$ °C), blue denotes cooling ($\Delta LST_{fc} < -0.02$ °C) and grey represents LST neutrality ($\Delta LST_{fc} = 0.0 \pm 0.02$ °C) induced by direct biophysical effects of tree cover gains and losses. The size of the dot indicates the degree of 1 s.e. The black dashed 1:1 lines represent equal fractions of tree cover gain and loss ($f_{gain} = f_{loss}$). The black solid curves, named LST-neutral curves, are fitted by quadratic models based on the scatter between f_{gain} and f_{loss} for grid cells with $\Delta LST_{fc} = 0.0 \pm 0.02$ °C (Methods), thereby separating the biophysical cooling and warming effects on LST. Shading represents the 95% confidence interval assessed by bootstrapping across each grid cell ($n = 500$). The significance (*P* value) of all fitted curves is <0.001. **j**–**l**, The average ΔLST_{fc} (means ± 2 s.e.) in disturbed forest grid cells with equivalent f_{gain} and f_{loss} ($f_{net} = 0 \pm 0.02$) for tropical (**j**, $n = 266$), temperate (**k**, $n = 296$) and boreal (**l**, $n = 151$) zones, respectively. The asterisks indicate probabilities statistically different from zero (two-sided Student's *t*-test): $^*P < 0.1$; $^{**}P < 0.05$; $^{***}P < 0.01$.

the distinct biophysical effects caused by gross tree cover gain and loss within LST grid cells.

To address this knowledge gap, we first selected forest grid cells that had undergone fine-scale gross tree cover changes while not changing land cover (hereafter referred to as subgrid tree cover gain and loss with respect to the coarser-scale LST observations), based on the Moderate Resolution Imaging Spectroradiometer (MODIS) land cover product[38,39] and 30 m resolution tree cover maps from Global Forest Watch (GFW)[15]. We then used the 0.05° resolution MOD11C3 v.061 LST product[38] to calculate the LST anomaly between 2000 and 2012 for each forest grid cell. Finally, the LST anomaly of neighbouring undisturbed grid cells caused by climate variability alone (ΔLST_{cv}) was removed from the signals of disturbed grid cells to quantify the direct biophysical effects on LST (ΔLST_{fc}) caused by subgrid fractional tree cover gains (f_{gain}) and losses (f_{loss}) from 2000 to 2012, following the methodology of ref. 5 and adapted with more stringent criteria (Methods).

Net tree cover loss may show a cooling effect

We found that some disturbed forests that experienced a net tree cover loss were still associated with a biophysical cooling effect (Fig. 1a,b). This occurred especially in tropical and temperate forest grid cells that experienced large fractions of gross tree cover gain, such as in the eastern United States ($f_{net} = -0.01 \pm 0.004$, $f_{gain} = 0.13 \pm 0.003$, daily mean $\Delta LST_{fc} = -0.05 \pm 0.002$ °C), eastern Congo ($f_{net} = -0.05 \pm 0.003$, $f_{gain} = 0.06 \pm 0.002$, daily mean $\Delta LST_{fc} = -0.03 \pm 0.009$ °C) and subtropical southern China ($f_{net} = -0.02 \pm 0.003$, $f_{gain} = 0.06 \pm 0.003$, daily mean $\Delta LST_{fc} = -0.04 \pm 0.006$ °C) (Fig. 1a,b,e,f). This result is different from previous findings where deforestation was systematically associated with a biophysical warming[5,9,22,23]. This phenomenon occurred because, for the same value of f_{net}, the sign and magnitude of ΔLST_{fc} depended largely on the absolute values of f_{gain} (Supplementary Fig. 1). Therefore, we quantified the sensitivity of ΔLST_{fc} to a unit of gross tree cover gain (S_{gain}) and loss (S_{loss}) (Methods). For the global average, S_{gain} (-0.81 ± 0.024 °C) (Fig. 1c) was greater in absolute value than S_{loss} (0.66 ± 0.021 °C) (Fig. 1d). The difference in magnitude between S_{gain} and S_{loss} was typically remarkable in temperate and tropical zones, for instance, in the eastern United States ($S_{gain} = -0.76 \pm 0.037$ °C; $S_{loss} = 0.59 \pm 0.027$ °C), eastern Congo ($S_{gain} = -0.80 \pm 0.091$ °C; $S_{loss} = 0.53 \pm 0.095$ °C) and subtropical southern China ($S_{gain} = -0.98 \pm 0.098$ °C; $S_{loss} = 0.70 \pm 0.102$ °C) (Fig. 1c,d,g,h).

Asymmetric ΔLST_{fc} of tree cover gain and loss

The variations in ΔLST_{fc} in disturbed forest grid cells with all combinations of f_{gain} and f_{loss} are depicted in Fig. 2. In tropical and temperate forests, daytime ΔLST_{fc} was more negative (cooling) with increasing f_{gain} and more positive (warming) with increasing f_{loss} (Fig. 2a,b). Night time ΔLST_{fc} generally responded in the opposite manner (Fig. 2d,e) but with a smaller absolute value than daytime ΔLST_{fc}. Consequently, in tropical and temperate forests, the daily mean ΔLST_{fc} (Fig. 2g,h) was

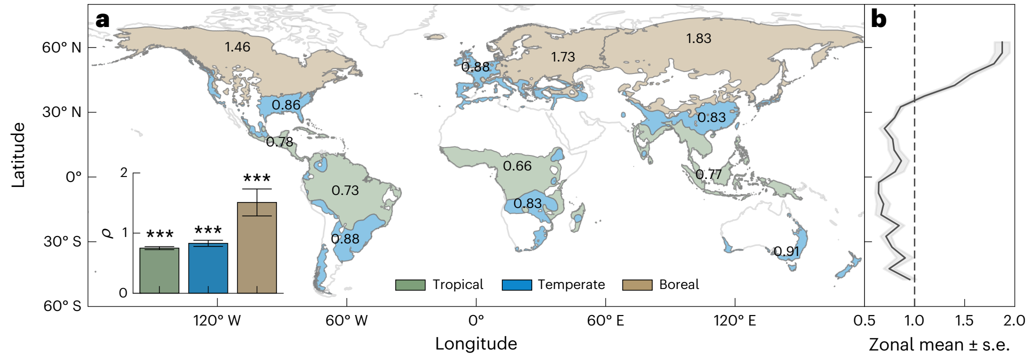

Fig. 3 | Ratio of fractional tree cover gain to loss for LST neutrality. a, The ratio (ρ) of fractional tree cover gain to loss (means ± s.e.) with daily mean ΔLST_{fc} = 0.0 ± 0.02 °C for the tropical (light green), temperate (light blue) and boreal (light brown) climate regions, respectively. The inset histograms in **a** represent ρ values (means ± s.e.) in the tropical (n = 2,048), temperate (n = 2,496) and boreal (n = 4,002) climate zones, respectively. The asterisks indicate probabilities statistically different from 1:1 (two-sided Student's t-test): $^{*}P < 0.1$, $^{**}P < 0.05$, $^{***}P < 0.01$. **b**, The zonal mean ρ values for each 5° latitude bins (medians ± s.e).

dominated by the daytime ΔLST_{fc} signal. In boreal forests, however, the daily mean ΔLST_{fc} (Fig. 2i) largely depended on night time ΔLST_{fc} (Fig. 2f), which had a greater magnitude than daytime ΔLST_{fc} (Fig. 2c). The daily mean ΔLST_{fc} in this biome was more positive (warming) with increasing f_{gain} and more negative (cooling) with increasing f_{loss} (Fig. 2i).

Interestingly, results indicate that the warming and cooling on LST induced by direct biophysical effects of tree cover changes were not symmetrically distributed along the 1:1 diagonal line defining $f_{gain} = f_{loss}$ (Fig. 2). The relationship between f_{gain} and f_{loss} for disturbed forest grid cells that result in net-zero change in LST (ΔLST_{fc} = 0 ± 0.02 °C, hereafter referred to as LST neutrality) can be approximated using a quadratic function, $f_{gain} = q(f_{loss})$ (Methods), illustrated by the black solid curves in Fig. 2 (here referred to as the LST-neutral curves). In tropical and temperate forests, this quadratic function laid below the 1:1 diagonal line, indicating a negative asymmetry of f_{gain} on biophysical LST neutrality (Fig. 2a,b,d,e,g,h). Consequently, the grid cells with $f_{gain} = f_{loss}$ were associated with a daytime cooling effect (tropical −0.58 ± 0.009 °C; temperate −0.33 ± 0.004 °C) and a small night time warming effect (tropical 0.07 ± 0.005 °C; temperate 0.05 ± 0.002 °C), leading to an overall cooling effect on the daily mean LST (tropical −0.25 ± 0.007 °C; temperate −0.14 ± 0.003 °C) (Fig. 2j,k). Conversely, in boreal forests, the q function was above the 1:1 line, implying a positive asymmetry of f_{gain} on biophysical LST neutrality (Fig. 2c,f,i). Grid cells with $f_{gain} = f_{loss}$ showed a warming effect on daytime LST (0.07 ± 0.002 °C) and a stronger cooling effect on night time LST (−0.11 ± 0.002 °C), resulting in a slight cooling effect on the daily mean LST (−0.02 ± 0.002 °C) (Fig. 2l). Additionally, these asymmetric responses of ΔLST_{fc} with respect to f_{gain} versus f_{loss} were still robust to the choice of another time period (2003–2012, 2006–2012 and 2009–2012), for larger LST grid-cell sizes (0.1° instead of 0.05°) and under different thresholds of final tree cover for estimating f_{gain} in disturbed forests (Supplementary Figs. 2–6 and Methods).

To quantify the asymmetry influences of f_{gain} versus f_{loss} on LST, we calculated the ratio of f_{gain} to f_{loss}, hereafter referred to as ρ, in disturbed grid cells with biophysical LST neutrality (daily mean ΔLST_{fc} = 0.0 ± 0.02 °C). Around the globe, ρ showed a distinctive latitudinal gradient (Fig. 3 and Supplementary Fig. 7). In tropical forests, ρ had the smallest values, that is, <1.0 (average ρ = 0.75 ± 0.025) (Fig. 3a), suggesting that lower gains in tree cover than losses can achieve LST neutrality for this biome. Within tropical forest regions, ρ was smaller in tropical Africa than in tropical South America and tropical Asia. In temperate forests, the value of ρ was larger than that of tropical forests (average ρ = 0.83 ± 0.051) (Fig. 3a) and increased with latitude (Fig. 3b). In boreal forests, ρ mostly varied between 1.0 and 2.0 (average ρ = 1.51 ± 0.224) and was the highest in Siberia (Fig. 3a). In this biome, if only the direct biophysical effect was considered, the ratio of f_{gain} to f_{loss} would be smaller than ρ to achieve a negative LST anomaly.

Mechanisms of the asymmetrical effects on LST

The asymmetric responses of ΔLST_{fc} with respect to f_{gain} and f_{loss} can be explained by the asymmetric influences of tree cover gain versus loss on the surface energy balance[7,40–44] (Fig. 4a–l and Supplementary Fig. 8), which were diagnosed using satellite observations of albedo, shortwave downwelling radiation (SW) and latent heat (LE) turbulent fluxes (Methods).

In the tropical and temperate forests, the neutral curves for changes in the surface energy fluxes were all below the 1:1 diagonal line in the (f_{gain},f_{loss}) spaces (Fig. 4a,b,d,e,g,h,j,k). Disturbed tropical forests with $f_{gain} = f_{loss}$ showed lower values of reflected SW (albedo multiplied by incoming SW) (ΔSW = −0.9 ± 0.2 W m^{-2}) (Fig. 4m), higher values of LE (ΔLE = 5.1 ± 0.4 W m^{-2}) (Fig. 4n) and small increases in sensible heat and ground heat fluxes ($\Delta(H+G)$ = 0.2 ± 0.1 W m^{-2}) (Fig. 4o) compared with undisturbed forests. Overall, these processes caused a net decrease in surface energy budget (ΔLW = −4.4 ± 0.2 W m^{-2}) (Fig. 4p), which explained the cooling signal shown in Fig. 2. In temperate forests, the grid cells with $f_{gain} = f_{loss}$ showed a moderate cooling effect, indicated by a moderate reduction in SW reflection (ΔSW = −0.5 ± 0.1 W m^{-2}) (Fig. 4m), a moderate increase in LE (ΔLE = 2.0 ± 0.2 W m^{-2}) and H and G fluxes ($\Delta(H+G)$ = 0.4 ± 0.1 W m^{-2}) (Fig. 4o). In these two biomes, the stronger increase in evapotranspiration (ET) associated with tree cover gain compared to the decrease from tree cover loss was the main cause of the negative asymmetry of f_{gain} on ΔLST_{fc} in the disturbed forests, where tree cover losses were mainly induced by commodity-driven deforestation, shifting agriculture and forestry[40] (inset histograms in Fig. 4a,b,d,e,g,h,j,k; Supplementary Figs. 9–14). This is because the young trees associated with tree cover gain are usually shorter and have higher leaf water potential and a consequent larger ET than the previous tree cover[45–49]. In contrast, the changes in reflected SW induced by albedo differences were negligible between newly grown young trees and previously lost older trees[42,43]. These processes eventually led to a negative asymmetric influence of tree cover gain versus loss on ΔLST_{fc} (Fig. 2). By matching GFW data[15] with planting years from a global map of plantations[50] (Methods), we show that the LST-neutral curves for plantations older than 6 years were slightly more distant from the 1:1 diagonal lines than those of younger plantations (Fig. 5a,b), indicating that tree age is one vital factor influencing the asymmetry of f_{gain} versus f_{loss} on ΔLST_{fc}. A space-for-time analysis over a longer period

https://doi.org/10.1038/s41558-023-01757-7

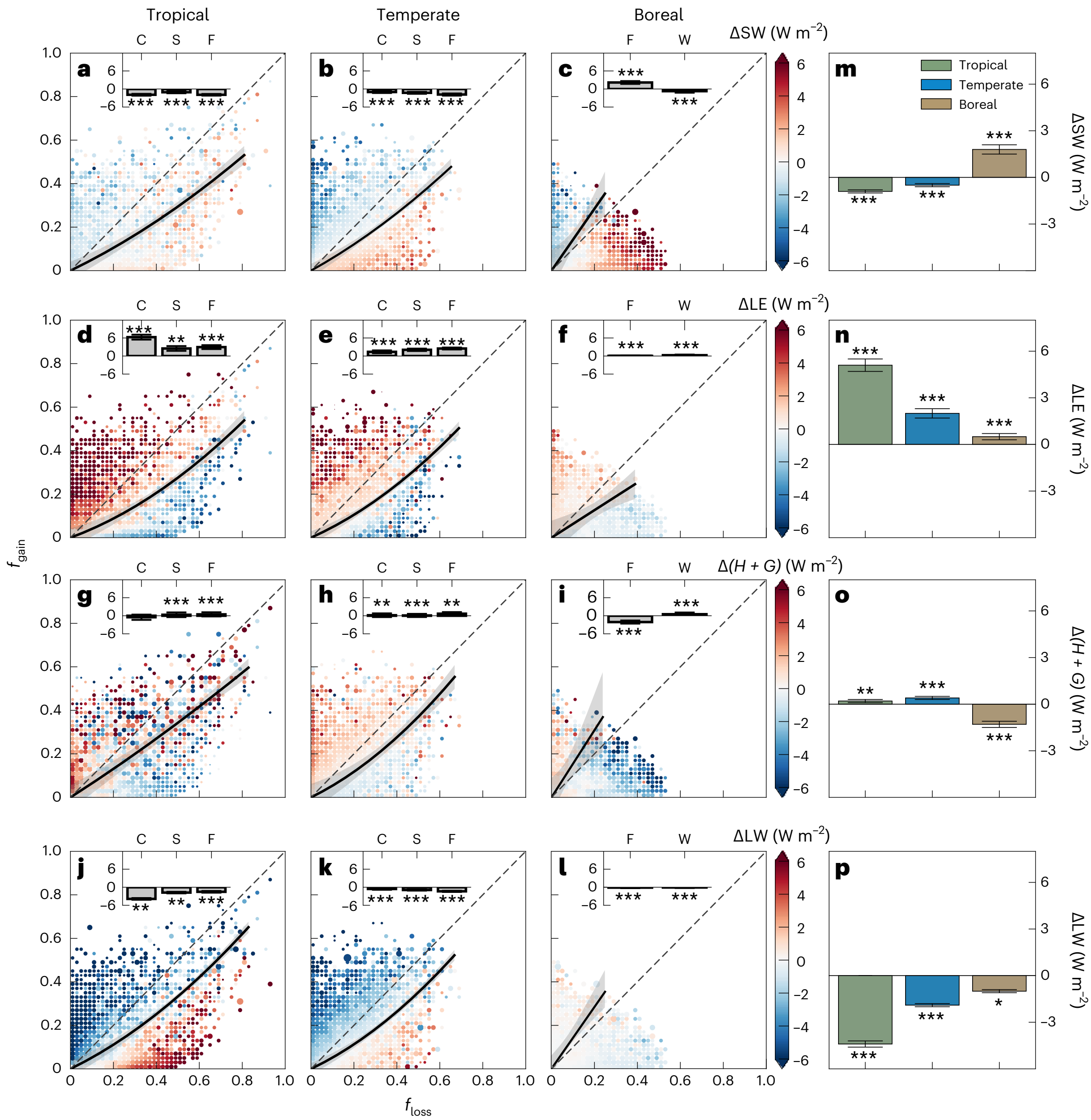

Fig. 4 | Asymmetric influences of tree cover gain and loss on surface energy balance. a–l, Bubble matrix plots of ΔSW (**a**–**c**), ΔLE (**d**–**f**), Δ(H + G) (**g**–**i**) and ΔLW (**j**–**l**) against various f_{gain} and f_{loss} in tropical (**a**,**d**,**g**,**j**), temperate (**b**,**e**,**h**,**k**) and boreal (**c**,**f**,**i**,**l**) zones, respectively. The Δ symbol stands for the difference between disturbed and undisturbed forests. Each cell in the bubble matrix shows the mean value of each energy flux component for a given combination of f_{loss} and f_{gain} in 0.05° pixels on the x and y axes in the 0.02 bin, respectively. Red indicates a positive value, blue indicates a negative value and grey indicates a value of zero. The size of the dot indicates the degree of 1 s.e. The black dashed 1:1 diagonal lines represent equal values of tree cover gain and loss ($f_{gain} = f_{loss}$). The neutral curves are fitted by quadratic models based on the scatters between f_{gain} and f_{loss}, similar to the LST-neutral curves in Fig. 2. Shading represents the 95% confidence interval assessed by bootstrapping across each pixel (n = 500). The significance (P value) of all fitted curves is <0.001. **m**–**p**, The average anomaly of each component (ΔSW (**m**), ΔLE (**n**), Δ(H + G) (**o**) and ΔLW (**p**)) (means ± s.e.) in the surface energy balance induced by tree cover changes with equivalent f_{gain} and f_{loss} ($f_{net} = 0 \pm 0.02$) for tropical (n = 266), temperate (n = 296) and boreal (n = 151) zones, respectively. Further details for forest grid cells disturbed by different drivers are graphed as inset histograms in **a**–**l**. C, S, F and W denote commodity-driven deforestation, shifting agriculture, forestry and wildfire, respectively. The asterisks indicate probabilities statistically different from zero (two-sided Student's t-test): *P < 0.1, **P < 0.05, ***P < 0.01. More details are shown in Supplementary Figs. 12–14.

indicated that direct biophysical cooling of plantations on LST diminished as planted trees became older than approximately 28 years in tropical regions and 32 years in temperate regions (Fig. 5c). This result implies that influences of tree age on asymmetric patterns of ΔLST_{fc} may become weaker when trees exhibit lower growth rates[51] (Methods).

In boreal forests, the situation is different. The neutral curves in the (f_{gain}, f_{loss}) spaces were above the 1:1 diagonal line for ΔSW and Δ(H + G) and below the 1:1 diagonal line for ΔLE (Fig. 4c,f,i). Disturbed grid cells in which $f_{gain} = f_{loss}$ were associated with a large increase in reflected SW (ΔSW = 1.8 ± 0.3 W m^{-2}) (Fig. 4m), a small increase in LE (ΔLE = 0.5 ± 0.2 W m^{-2}) (Fig. 4n) and a strong decrease in H and G (Δ(H + G) = −1.3 ± 0.2 W m^{-2}) (Fig. 4o). These processes resulted in a minor decrease in the surface energy budget (ΔLW = −1.0 ± 0.1 W m^{-2}) (Fig. 4l,p) and thus a negligible biophysical cooling effect (Fig. 2). Therefore, the change in SW was the main cause for the asymmetric changes in the surface energy balance caused by tree cover gain versus loss, whereas tree age-induced ET changes played a less important role. The stronger contribution of SW changes in boreal forests was mainly attributed to the lower forest albedo during snow-covered periods[6,52–54], typically 20% to 50% less than in snow-covered open areas.

https://doi.org/10.1038/s41558-023-01757-7

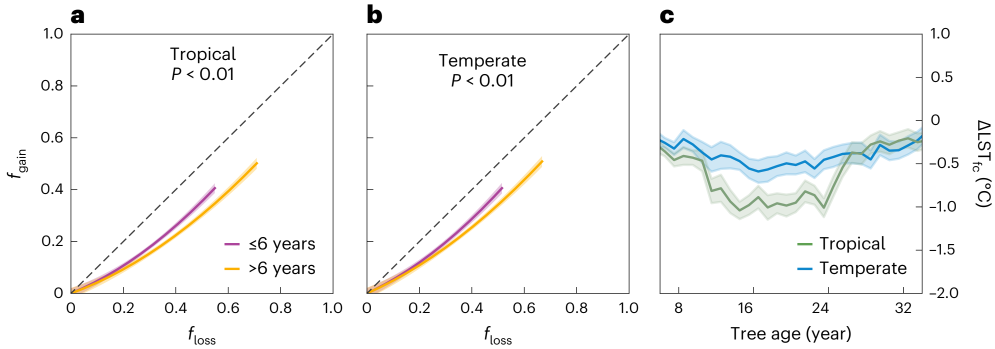

Fig. 5 | Influences of tree age on the asymmetric temperature effects of tree cover gain and loss. a,**b**, LST-neutral curves for disturbed forest grid cells with different planting ages (purple, planting age ≤ 6 years; orange, planting age > 6 years) in tropical (**a**) and temperate (**b**) zones. The LST-neutral curves are fitted by quadratic models (Supplementary Figs. 15 and 16). Shading represents the 95% confidence interval assessed by bootstrapping across each pixel ($n = 500$). The *P* values in **a**,**b** are probabilities statistically different between the two planting age groups (one-sided *f*-test). **c**, Variations in the daily mean ΔLST_{fc} (means ± s.e) along with tree age (bin times: 1 year) in planted forests. Tree age influences ΔLST_{fc} in planted forests with different tree covers ($50\% < f_{gain} \leq 70\%$ versus $f_{gain} > 70\%$), as shown in Supplementary Fig. 17.

In addition, the dominant coniferous forests in the boreal region[13] were typically darker (lower albedo)[6] than broadleaved trees prevailing elsewhere[55,56]. Forestry and wildfire were the two dominant causes of tree cover losses in disturbed boreal forests (inset histogram in Fig. 4c,f,i,l; Supplementary Figs. 9–14). However, standing dead trees at recently burnt sites only partially masked winter snow cover and led to a weaker albedo increase than from timber harvest[7,18], which caused a strong increase in the reflected SW for forestry compared to wildfire (Fig. 4c and Supplementary Fig. 12). Therefore, forestry-induced net changes in SW seem to be the main driver of the asymmetric response of ΔLST_{fc} in boreal forests where $f_{gain} = f_{loss}$. This finding is consistent with previous studies[5,24,42,57] that showed that albedo-induced net change in SW was the major cause of the change in direct biophysical effects on LST over boreal forests.

To assess the uncertainties of satellite-based retrievals of the surface energy balance, in addition to the MODIS ET dataset[58] used above, we tested two alternative datasets: the 0.05° resolution ET data products from Global Land Surface Satellite (GLASS)[59] and Penman-Monteith-Leuning (PML_v2) ET[60]. These two different ET datasets (Supplementary Fig. 18) showed marginally small differences compared with those derived from MODIS ET (Supplementary Fig. 8d–f), confirming the robustness of the explanations for the observed asymmetry patterns of ΔLST_{fc}.

Uncertainties from tree cover change data

Previous studies indicate that potential uncertainties exist in some regions (such as Canada, China and Brazil) in the GFW tree cover data[61–64]. Here, we used tree cover maps from individual countries or regions including Canada[65], the United States[66], eastern Europe[67], northern Europe[68], China[69] and tropical moist forests[70] (Supplementary Table 2 and Supplementary Fig. 19), which were calibrated or validated using national forest cover statistics or field inventory data[71] (Supplementary Fig. 20), as a means to provide an alternative data source for tree cover gain and loss[72].

In temperate forests, as in the United States, both f_{gain} and f_{loss} agreed well with those from the National Land Cover Database (NLCD)[66] (Supplementary Fig. 21) and the ρ difference ($\Delta\rho$) for the LST-neutral curves between NLCD and GFW tree cover data was approximately equal to zero. However, an underestimation of tree cover gains often occurred in regions with large afforestation programs such as China[22]. Thus, the negative asymmetry of f_{gain} on LST neutrality in China from GFW data was weakened ($\Delta\rho = 0.07 \pm 0.019$) but the LST-neutral curves from regional data were still below the 1:1 diagonal line (Supplementary Fig. 22). In tropical moist forests, the lower performance of GFW tree cover data mainly stemmed from an overestimation of tree cover compared with an underestimation in dry tropical forests[73–75]. Our analyses showed that 68% of disturbed pixels in GFW tree cover data had a lower value of f_{loss}, 10% smaller than the regional data from the Joint Research Centre[70]. The negative asymmetry of f_{gain} on LST neutrality for this biome was to some extent underestimated in GFW tree cover data ($\Delta\rho = -0.07 \pm 0.008$) (Supplementary Fig. 23).

The situations differ in boreal forests. In eastern Europe, f_{gain} and f_{loss} of GFW tree cover data were almost equally underestimated compared with more accurate regional data from the Global Land Analysis and Discovery Laboratory[67] and the asymmetry patterns of ΔLST_{fc} changed marginally ($\Delta\rho = 0.03 \pm 0.001$) (Supplementary Fig. 24). However, in countries such as Norway, Finland and Sweden with a low sun angle and often cloudy weather[76] and where much of the non-clear-cutting harvest activities took place in small and irregular areas[77], GFW tree cover data probably had a lower f_{loss} compared with regional data from the Copernicus Land Monitoring Service[78,79] (Supplementary Fig. 25a–c). In contrast, in the boreal region of Canada with widespread low-density tree communities[80] and wildfire losses in less productive forests that require long recovery times[81], GFW tree cover data probably underestimated f_{gain} compared with data from the National Terrestrial Ecosystem Monitoring System[65] (Supplementary Fig. 26a–c). Results indicated a weaker positive asymmetry of f_{gain} on LST neutrality in northern Europe ($\Delta\rho = -0.12 \pm 0.010$) but a stronger one in Canada ($\Delta\rho = 0.07 \pm 0.023$) (**d**–**i** in Supplementary Figs. 25 and 26).

Discussion

The most challenging aspect for quantifying the direct biophysical effects of forests lies in effectively removing the influences from climate variability[5,36]. Others[5] selected forest grid cells that experienced net-zero changes in forest cover and attributed their LST anomalies to climate variability. However, we highlighted an asymmetric effect of tree cover gain versus loss on LST so that forest grid cells with net-zero change in tree cover may lead to either a negative or positive LST anomaly, highly depending on the background climate and tree biophysical properties. Therefore, an optimal reference should be selected from undisturbed forests with no gross tree cover gain and loss.

Second, satellite- and ground-based estimations of the direct biophysical effects of forests have shown inconsistencies in both sign and magnitude[13,24,42]. It has been argued that satellite-based LST (skin temperature)[5,12,13,24,82] is more sensitive to aerodynamic resistance[5,42,44] associated with forest cover changes than the ground-based, near-surface air temperature[7,12,23,83,84]. Our finding can provide an alternative explanation. Satellite-based LST usually samples a land pixel which represents the mixed biophysical LST effects of subgrid gross tree cover gains and losses. In contrast, tower studies have a smaller footprint and sample small forest stands[50,85,86]. This mismatch in spatial scales was mostly neglected in previous studies, which simplified that the temperature differences between paired sites were explained solely by net differences in forest cover[42].

Finally, while many satellite tree cover data are regionally validated, a comprehensive validation using field inventory tree cover data remains challenging[63,64]. One important discrepancy between satellite-based and field inventory tree cover data is probably driven by forest management activities which result in changes in tree cover but not in land cover[71]. It is also important to recognize that the direct biophysical temperature effect analysed in this study is different from the full climate impacts, involving both indirect biophysical[87] and biogeochemical effects[88] which could either dampen or amplify surface temperature change[89,90].

In conclusion, we provide a global estimate of direct biophysical effects of gross tree cover gain and loss at fine resolution and demonstrate an asymmetric effect of tree cover gain versus loss on LST. We also quantify an average ratio of tree cover gain to loss to achieve a net direct biophysical cooling, which could be considered for climate-smart forest management. Our findings may have far-reaching implications for biodiversity, functional traits and ecosystem functioning, as they are strongly driven by local temperatures.

Online content

Any methods, additional references, Nature Portfolio reporting summaries, source data, extended data, supplementary information, acknowledgements, peer review information; details of author contributions and competing interests; and statements of data and code availability are available at https://doi.org/10.1038/s41558-023-01757-7.

References

1. Carvalhais, N. et al. Global covariation of carbon turnover times with climate in terrestrial ecosystems. *Nature* **514**, 213–217 (2014).
2. Le Quéré, C. et al. Global carbon budget 2013. *Earth Syst. Sci. Data* **6**, 235–263 (2014).
3. Friedlingstein, P. et al. Global carbon budget 2019. *Earth Syst. Sci. Data* **11**, 1783–1838 (2019).
4. Bonan, G. B. Forests and climate change: forcings, feedbacks, and the climate benefits of forests. *Science* **320**, 1444–1449 (2008).
5. Alkama, R. & Cescatti, A. Biophysical climate impacts of recent changes in global forest cover. *Science* **351**, 600–604 (2016).
6. Betts, R. A. Offset of the potential carbon sink from boreal forestation by decreases in surface albedo. *Nature* **408**, 187–190 (2000).
7. Lee, X. et al. Observed increase in local cooling effect of deforestation at higher latitudes. *Nature* **479**, 384–387 (2011).
8. Mahmood, R. et al. Land cover changes and their biogeophysical effects on climate. *Int. J. Climatol.* **34**, 929–953 (2014).
9. Zeng, Z. et al. Climate mitigation from vegetation biophysical feedbacks during the past three decades. *Nat. Clim. Change* **7**, 432–436 (2017).
10. Davin, E. L., de Noblet-Ducoudré, N. & Friedlingstein, P. Impact of land cover change on surface climate: relevance of the radiative forcing concept. *Geophys. Res. Lett.* **34**, L13702 (2007).
11. Windisch, M. G., Davin, E. L. & Seneviratne, S. I. Prioritizing forestation based on biogeochemical and local biogeophysical impacts. *Nat. Clim. Change* **11**, 867–871 (2021).
12. Bright, R. M. et al. Local temperature response to land cover and management change driven by non-radiative processes. *Nat. Clim. Change* **7**, 296–302 (2017).
13. Duveiller, G., Hooker, J. & Cescatti, A. The mark of vegetation change on Earth's surface energy balance. *Nat. Commun.* **9**, 679 (2018).
14. Xu, R. et al. Contrasting impacts of forests on cloud cover based on satellite observations. *Nat. Commun.* **13**, 670 (2022).
15. Hansen, M. C. et al. High-resolution global maps of 21st-century forest cover change. *Science* **342**, 850–853 (2013).
16. Sterling, S., Ducharne, A. & Polcher, J. The impact of global land-cover change on the terrestrial water cycle. *Nat. Clim. Change* **3**, 385–390 (2013).
17. Lejeune, Q., Davin, E. L., Gudmundsson, L., Winckler, J. & Seneviratne, S. I. Historical deforestation locally increased the intensity of hot days in northern mid-latitudes. *Nat. Clim. Change* **8**, 386–390 (2018).
18. Liu, Z., Ballantyne, A. P. & Cooper, L. A. Biophysical feedback of global forest fires on surface temperature. *Nat. Commun.* **10**, 214 (2019).
19. Claussen, M., Brovkin, V. & Ganopolski, A. Biogeophysical versus biogeochemical feedbacks of large-scale land cover change. *Geophys. Res. Lett.* **28**, 1011–1014 (2001).
20. Wang, J. et al. Temperature changes induced by biogeochemical and biophysical effects of bioenergy crop cultivation. *Environ. Sci. Technol.* **57**, 2474–2483 (2023).
21. Zhu, L. et al. Comparable biophysical and biogeochemical feedbacks on warming from tropical moist forest degradation. *Nat. Geosci.* **16**, 244–249 (2023).
22. Peng, S.-S. et al. Afforestation in China cools local land surface temperature. *Proc. Natl Acad. Sci. USA* **111**, 2915–2919 (2014).
23. Luyssaert, S. et al. Land management and land-cover change have impacts of similar magnitude on surface temperature. *Nat. Clim. Change* **4**, 389–393 (2014).
24. Li, Y. et al. Local cooling and warming effects of forests based on satellite observations. *Nat. Commun.* **6**, 6603 (2015).
25. Pickett, S. T. in *Long-Term Studies in Ecology: Approaches and Alternatives* (ed. Likens, G. E.) 110–135 (Springer, 1989).
26. Senf, C. & Seidl, R. Mapping the forest disturbance regimes of Europe. *Nat. Sustain.* **4**, 63–70 (2021).
27. Tong, X. et al. Forest management in southern China generates short term extensive carbon sequestration. *Nat. Commun.* **11**, 129 (2020).
28. Heinrich, V. H. et al. Large carbon sink potential of secondary forests in the Brazilian Amazon to mitigate climate change. *Nat. Commun.* **12**, 1785 (2021).
29. Ryan, M. G., Binkley, D. & Fownes, J. H. Age-related decline in forest productivity: pattern and process. *Adv. Ecol. Res.* **27**, 213–262 (1997).
30. Naudts, K. et al. Europe's forest management did not mitigate climate warming. *Science* **351**, 597–600 (2016).
31. Cooper, L. A., Ballantyne, A. P., Holden, Z. A. & Landguth, E. L. Disturbance impacts on land surface temperature and gross primary productivity in the western United States. *J. Geophys. Res. Biogeosci.* **122**, 930–946 (2017).
32. Randerson, J. T. et al. The impact of boreal forest fire on climate warming. *Science* **314**, 1130–1132 (2006).
33. Maness, H., Kushner, P. J. & Fung, I. Summertime climate response to mountain pine beetle disturbance in British Columbia. *Nat. Geosci.* **6**, 65–70 (2013).
34. O'Halloran, T. L. et al. Radiative forcing of natural forest disturbances. *Glob. Change Biol.* **18**, 555–565 (2012).
35. Rogers, B. M., Soja, A. J., Goulden, M. L. & Randerson, J. T. Influence of tree species on continental differences in boreal fires and climate feedbacks. *Nat. Geosci.* **8**, 228–234 (2015).
36. Zeng, Z. et al. Deforestation-induced warming over tropical mountain regions regulated by elevation. *Nat. Geosci.* **14**, 23–29 (2021).
37. Zhang, Y. & Liang, S. Impacts of land cover transitions on surface temperature in China based on satellite observations. *Environ. Res. Lett.* **13**, 024010 (2018).

38. Wan, Z., Hook, S. & Hulley, G. MODIS/Terra Land Surface Temperature/Emissivity Monthly L3 Global 0.05Deg CMG V061. *NASA EOSDIS Land Processes DAAC* https://doi.org/10.5067/MODIS/MOD11C3.061 (2021).
39. Friedl, M. & Sulla-Menashe, D. MODIS/Terra+Aqua Land Cover Type Yearly L3 Global 0.05Deg CMG V061. *NASA EOSDIS Land Processes DAAC* https://doi.org/10.5067/MODIS/MCD12C1.061 (2022).
40. Curtis, P. G., Slay, C. M., Harris, N. L., Tyukavina, A. & Hansen, M. C. Classifying drivers of global forest loss. *Science* **361**, 1108–1111 (2018).
41. Su, Y. et al. Quantifying the biophysical effects of forests on local air temperature using a novel three-layered land surface energy balance model. *Environ. Int.* **132**, 105080 (2019).
42. Lawrence, D., Coe, M., Walker, W., Verchot, L. & Vandecar, K. The unseen effects of deforestation: biophysical effects on climate. *Front. For. Glob. Change* **5**, 756115 (2022).
43. Davin, E. L. & de Noblet-Ducoudré, N. Climatic impact of global-scale deforestation: radiative versus nonradiative processes. *J. Clim.* **23**, 97–112 (2010).
44. Su, Y. et al. Aerodynamic resistance and Bowen ratio explain the biophysical effects of forest cover on understory air and soil temperatures at the global scale. *Agric. Meteorol.* **308**, 108615 (2021).
45. Malhi, Y., Baldocchi, D. D. & Jarvis, P. G. The carbon balance of tropical, temperate and boreal forests. *Plant Cell Environ.* **22**, 715–740 (1999).
46. Cook-Patton, S. C. et al. Mapping carbon accumulation potential from global natural forest regrowth. *Nature* **585**, 545–550 (2020).
47. Moore, G. W., Bond, B. J., Jones, J. A., Phillips, N. & Meinzer, F. C. Structural and compositional controls on transpiration in the 40- and 450-year-old riparian forests in western Oregon, USA. *Tree Physiol.* **24**, 481–491 (2004).
48. Jassal, R. S., Black, T. A., Spittlehouse, D. L., Brümmer, C. & Nesic, Z. Evapotranspiration and water use efficiency in different-aged Pacific Northwest Douglas-fir stands. *Agric. Meteorol.* **149**, 1168–1178 (2009).
49. Stoy, P. C. et al. Separating the effects of climate and vegetation on evapotranspiration along a successional chronosequence in the southeastern US. *Glob. Change Biol.* **12**, 2115–2135 (2006).
50. Du, Z. et al. A global map of planting years of plantations. *Sci. Data* **9**, 141 (2022).
51. Aryal, D. R., De Jong, B. H. J., Ochoa-Gaona, S., Esparza-Olguin, L. & Mendoza-Vega, J. Carbon stocks and changes in tropical secondary forests of southern Mexico. *Agric. Ecosyst. Environ.* **195**, 220–230 (2014).
52. Potter, S. et al. Climate change decreases the cooling effect from postfire albedo in boreal North America. *Glob. Change Biol.* **26**, 1592–1607 (2020).
53. He, T., Liang, S. & Song, D. X. Analysis of global land surface albedo climatology and spatial-temporal variation during 1981–2010 from multiple satellite products. *J. Geophys. Res. Atmos.* **119**, 281–298 (2014).
54. Gao, F. et al. Multiscale climatological albedo look-up maps derived from MODIS BRDF/albedo products. *J. Appl. Remote Sens.* **8**, 083532 (2014).
55. Baldocchi, D., Kelliher, F. M., Black, T. A. & Jarvis, P. Climate and vegetation controls on boreal zone energy exchange. *Glob. Change Biol.* **6**, 69–83 (2000).
56. Oris, F., Asselin, H., Ali, A. A., Finsinger, W. & Bergeron, Y. Effect of increased fire activity on global warming in the boreal forest. *Environ. Rev.* **22**, 206–219 (2014).
57. Anderson, R. G. et al. Biophysical considerations in forestry for climate protection. *Front. Ecol. Environ.* **9**, 174–182 (2011).
58. Running, S., Mu, Q., Zhao, M. & Moreno, A. MODIS/Terra Net Evapotranspiration Gap-Filled Yearly L4 Global 500m SIN Grid V061. *NASA EOSDIS Land Processes DAAC* https://doi.org/10.5067/MODIS/MOD16A3GF.061 (2021).
59. Yao, Y. J. et al. MODIS-driven estimation of terrestrial latent heat flux in China based on a modified Priestley–Taylor algorithm. *Agric. Meteorol.* **171**, 187–202 (2013).
60. Zhang, Y. et al. Coupled estimation of 500m and 8-day resolution global evapotranspiration and gross primary production in 2002–2017. *Remote Sens. Environ.* **222**, 165–182 (2019).
61. Tropek, R. et al. Comment on "High-resolution global maps of 21st-century forest cover change". *Science* **344**, 981–981 (2014).
62. Milodowski, D. T., Mitchard, E. T. A. & Williams, M. Forest loss maps from regional satellite monitoring systematically underestimate deforestation in two rapidly changing parts of the Amazon. *Environ. Res. Lett.* **12**, 094003 (2017).
63. Breidenbach, J. et al. Harvested area did not increase abruptly—how advancements in satellite-based mapping led to erroneous conclusions. *Ann. For. Sci.* **79**, 2 (2022).
64. Ogle, S. M. et al. Delineating managed land for reporting national greenhouse gas emissions and removals to the United Nations framework convention on climate change. *Carbon Balance Manag.* **13**, 9 (2018).
65. Hermosilla, T. et al. Mass data processing of time series Landsat imagery: pixels to data products for forest monitoring. *Int. J. Digit. Earth.* **9**, 1035–1054 (2016).
66. Dewitz, J. *National Land Cover Database (NLCD) 2019 Products (Ver. 2.0, June 2021)* (US Geological Survey, 2021).
67. Potapov, P. V. et al. Eastern Europe's forest cover dynamics from 1985 to 2012 quantified from the full Landsat archive. *Remote Sens. Environ.* **159**, 28–43 (2015).
68. European Union. Change Maps. *Copernicus Land Monitoring Service* https://land.copernicus.eu/pan-european/high-resolution-layers/forests/tree-cover-density/change-maps (2023).
69. Guo, J., Gong, P., Dronova, I. & Zhu, Z. Forest cover change in China from 2000 to 2016. *Int. J. Remote Sens.* **43**, 593–606 (2022).
70. Vancutsem, C. et al. Long-term (1990–2019) monitoring of forest cover changes in the humid tropics. *Sci. Adv.* **7**, eabe1603 (2021).
71. Barrett, F., McRoberts, R. E., Tomppo, E., Cienciala, E. & Waser, L. T. Remote sensing of environment: a questionnaire-based review of the operational use of remotely sensed data by national forest inventories. *Remote Sens. Environ.* **174**, 279–289 (2016).
72. McRoberts, R. E. et al. Using a finer resolution biomass map to assess the accuracy of a regional, map-based estimate of forest biomass. *Surv. Geophys.* **40**, 1001–1015 (2019).
73. Cunningham, D., Cunningham, P. & Fagan, M. E. Identifying biases in global tree cover products: a case study in Costa Rica. *Forests* **10**, 853 (2019).
74. Sannier, C., McRoberts, R. E. & Fichet, L. V. Suitability of global forest change data to report forest cover estimates at national level in Gabon. *Remote Sens. Environ.* **173**, 326–338 (2016).
75. Hojas-Gascon, L., Cerutti, P. O., Eva, H., Nasi, R. & Martius, C. *Monitoring Deforestation and Forest Degradation in the Context of REDD+: Lessons from Tanzania* (CIFOR, 2015).
76. Pitkänen, T. P. et al. Errors related to the automatized satellite-based change detection of boreal forests in Finland. *Int. J. Appl. Earth. Obs. Geoinf.* **86**, 102011 (2020).
77. Jutras-Perreault, M. C., Gobakken, T. & Ørka, H. O. Comparison of two algorithms for estimating stand-level changes and change indicators in a boreal forest in Norway. *Int. J. Appl. Earth. Obs. Geoinf.* **98**, 102316 (2021).
78. Palahí, M. et al. Concerns about reported harvests in European forests. *Nature* **592**, E15–E17 (2021).

79. Chirici, G. et al. Monitoring clearcutting and subsequent rapid recovery in Mediterranean coppice forests with Landsat time series. *Ann. For. Sci.* **77**, 40 (2020).
80. Timoney, K. P. & Mamet, S. No treeline advance over the last 50 years in subarctic western and central Canada and the problem of vegetation misclassification in remotely sensed data. *Écoscience* **27**, 93–106 (2020).
81. Guindon, L. et al. Missing forest cover gains in boreal forests explained. *Ecosphere* **9**, e02094 (2018).
82. Prevedello, J. A., Winck, G. R., Weber, M. M., Nichols, E. & Sinervo, B. Impacts of forestation and deforestation on local temperature across the globe. *PLoS ONE* **14**, e0213368 (2019).
83. Vanden, B. S., Luyssaert, S., Davin, E. L., Janssens, I. & van Lipzig, N. New insights in the capability of climate models to simulate the impact of LUC based on temperature decomposition of paired site observations. *J. Geophys. Res. Atmos.* **120**, 5417–5436 (2015).
84. Liao, W., Rigden, A. J. & Li, D. Attribution of local temperature response to deforestation. *J. Geophys. Res. Biogeosci.* **123**, 1572–1587 (2018).
85. George-Chacón, S. P., Mas, J. F., Dupuy, J. M., Castillo-Santiago, M. A. & Hernández-Stefanoni, J. L. Mapping the spatial distribution of stand age and aboveground biomass from Landsat time series analyses of forest cover loss in tropical dry forests. *Remote Sens. Ecol. Conserv.* **8**, 347–361 (2022).
86. Schultz, N. M., Lawrence, P. J. & Lee, X. Global satellite data highlights the diurnal asymmetry of the surface temperature response to deforestation. *J. Geophys. Res. Biogeosci.* **122**, 903–917 (2017).
87. Duveiller, G. et al. Revealing the widespread potential of forests to increase low level cloud cover. *Nat. Commun.* **12**, 4337 (2021).
88. Duveiller, G. et al. Biomass resilience of Neotropical secondary forests. *Nature* **530**, 211–214 (2016).
89. Meier, R. et al. Empirical estimate of forestation-induced precipitation changes in Europe. *Nat. Geosci.* **14**, 473–478 (2021).
90. Seidl, R., Schelhaas, M. J., Rammer, W. & Verkerk, P. J. Increasing forest disturbances in Europe and their impact on carbon storage. *Nat. Clim. Change* **4**, 806–810 (2014).

https://doi.org/10.1038/s41558-023-01757-7

Methods

Calculating the fraction of tree cover change

As an initial step, we overlaid the 30 m high-resolution global tree cover change maps from GFW[15] onto 0.05° resolution MODIS MCD12C1 land cover images[39] and selected the grid cells that were defined as 'forest-lands' in the MODIS land cover images. We then calculated the fractions of tree cover gain (f_{gain}) and tree cover loss (f_{loss}) for each 0.05° forest grid cell from 2000 to 2012.

GFW maps recorded three types of pixel—tree cover gain, loss and both[15]—with tree cover fraction information for 30 m resolution pixels in 2000. We estimated f_{gain} and f_{loss} for the 0.05° forest grid cells in 2012 by taking 2000 as the benchmark year. Overall, three cases were considered. (1) In a 0.05° resolution forest grid cell k, for pixel i labelled only 'forest loss' in GFW 30 m resolution maps, the tree cover decreased from the fraction (f_i^{30m}) in 2000 to zero by 2012; this is a direct estimate of f_{loss} using GFW tree cover data. (2) For pixel j labelled only 'forest gain', we assumed that the tree cover would increase to the average values ($f_{ref,j}{}^{30m}$) of neighbouring well-grown forests (surrounding 9 × 9 pixels) with tree cover fractions >50%. To verify this assumption, we compared the tree cover fraction[50] of a forest planted from 1982 to 2000 to the tree cover fractions of well-grown forests (9 × 9 pixels) surrounding that planted forest. The results show that the fractions were strongly and linearly correlated along the 1:1 diagonal line (all R^2 values >0.98; Supplementary Fig. 27). (3) For pixel z with both tree cover gains and losses, we assumed that the tree cover would initially decrease from the fraction (f_z^{30m}) in 2000 to zero, as did the pixels labelled only 'forest loss'. Then, we assumed that the tree cover fractions would increase to the average fraction ($f_{ref,z}{}^{30m}$) of surrounding well-grown forests in 2012, similar to pixels labelled only 'forest gain'. Thus, the average fraction of tree cover losses ($f_{loss,k}{}^{0.05°}$) and gains ($f_{gain,k}{}^{0.05°}$) for forest grid cell k was calculated using equations (1) and (2), respectively:

$$f_{\mathrm{loss},k}^{0.05°} = \left[\sum_{1}^{i}\left(f_i^{30m}\right) + \sum_{1}^{z}\left(f_z^{30m}\right)\right] \times \frac{0.00025 \times 0.00025}{0.05 \times 0.05} \quad (1)$$

$$f_{\mathrm{gain},k}^{0.05°} = \left[\sum_{1}^{j}\left(f_{\mathrm{ref},j}^{30m} - f_j^{30m}\right) + \sum_{1}^{z}\left(f_{\mathrm{ref},z}^{30m}\right)\right] \times \frac{0.00025 \times 0.00025}{0.05 \times 0.05} \quad (2)$$

where $f_{gain,k}^{0.05°}$ and $f_{loss,k}^{0.05°}$ denote the fractions of tree cover gains and tree cover losses for the 0.05° forest grid cell k, respectively. Parameter f_i^{30m} represents the tree cover fraction of the 30 m (~0.00025°) resolution grid i within the 0.05° forest grid k in 2000. Parameter $f_{ref}{}^{30m}$ represents the average tree cover fraction of surrounding 9 × 9 30 m resolution pixels with tree cover fractions >50% around the target pixel in 2000. Variables i and j denote the number of 30 m resolution pixels labelled as only forest gains and losses, respectively. Variable z denotes the number of 30 m resolution pixels that experienced both forest gains and losses. The conversion coefficient $\frac{0.00025\times0.00025}{0.05\times0.05}$ is the ratio of the spatial resolution in GFW tree cover maps to that of the MODIS MCD12C1 land cover maps.

Estimating ΔLST_{fc} caused by tree cover change

We used the 0.05° resolution MOD11C3 v.061 daytime and night time LST products[38] (referring to the skin temperature of land surfaces[5,7,38,42]) to represent the daytime and night time LST, respectively, and calculated the daily mean LST by averaging the MODIS daytime and night time LST. As the temperature anomaly (ΔLST_{total}) between two years in a given disturbed forest grid cell was the combined effect induced by both tree cover change and climate variability[5], we used the time-series analysis methodology developed by ref. 5 (equation (3)) to disentangle the direct biophysical effect of tree fractional gain and loss (ΔLST_{fc}) from that due to climate variability (ΔLST_{cv}).

In the method of ref. 5, forest grid cells with $f_{net} = 0 \pm 0.02$ were defined as reference undisturbed forests for estimating ΔLST_{cv}. In our methods, more stringent criteria were used to constrain the disturbed and undisturbed grid cells. We classified a forest grid cell as 'disturbed' if it experienced >2% of subgrid change in tree cover gain ($f_{gain} > 0.02$) or loss ($f_{loss} > 0.02$) based on 30 m resolution tree cover maps from GFW[15] from 2000 to 2012. Correspondingly, we classified a forest grid cell as 'undisturbed' if it experienced <2% of gross tree cover change ($f_{gain} \leq 0.02$ and $f_{loss} \leq 0.02$) and showed a stable normalized difference vegetation index ($\Delta NDVI = 0 \pm 0.02$). Overall, 34.7% of all the 0.05° forest grid cells were classified as disturbed forests, with 10.3% located in tropical regions, 6.8% in temperate regions and 17.6% in boreal regions (Fig. 1a). Approximately 57.4% of these disturbed forest grid cells, mainly in tropical (20° N–20° S) and boreal regions (Canada and eastern Russia), experienced a net tree cover loss defined by $f_{net} = f_{gain} - f_{loss} < -0.02$. Conversely, only 19.1% of the disturbed forests experienced net gains ($f_{net} > 0.02$), with these forests located mostly in Europe, western Russia and southern Brazil. The remaining 23.5% of the disturbed forests showed no net change in tree cover ($f_{net} = 0 \pm 0.02$).

For a certain disturbed forest grid cell, its reference grid cells were detected from neighbouring undisturbed forests located within a distance of 50 km (ref. 5), as grid cells within 50 km were assumed to share the most similar climate background[24]. We then took the temperature anomalies of reference undisturbed grid cells between 2000 and 2012 as those induced by climate variability without the interference of tree cover changes ($\Delta LST_{fc} \approx 0$ and $\Delta LST_{total} = \Delta LST_{cv}$). To limit the influence caused by distance, all ΔLST_{cv} values within 50 km of the disturbed forest grid cells were averaged using the inverse distance as a weighting factor, as shown in equation (4) (ref. 5). In addition, only those disturbed grid cells with more than five reference undisturbed grid cells within a 50 km distance[5] were included in the analysis.

$$\Delta LST_{fc} = \Delta LST_{total} - \Delta LST_{cv} \quad (3)$$

$$\Delta LST_{cv} = \frac{\sum_{k=1}^{n} \frac{\Delta LST_k}{d_k}}{\sum_{k=1}^{n} \frac{1}{d_k}} \quad (4)$$

where ΔLST_{total} (°C) signifies the overall LST change in disturbed forest grid cells; ΔLST_{fc} (°C) denotes the LST change in disturbed forest grid cells caused by tree cover gains and losses; ΔLST_{cv} (°C) is the LST change induced by climate variability; ΔLST_k (°C) denotes the LST changes in reference undisturbed forest grid cells (k) and d_k is the distance between the disturbed and undisturbed forest grid cells (k) in km.

We further quantified the sensitivity of ΔLST_{fc} to the fraction of tree cover gain (f_{gain}) and tree cover loss (f_{loss}) with a linear regression model as follows:

$$\Delta LST_{fc} = S_{gain} \times f_{gain} + S_{loss} \times f_{loss} \quad (5)$$

where S_{gain} (°C) and S_{loss} (°C) express the sensitivities of ΔLST_{fc} to f_{gain} and f_{loss}, respectively. Here, grid cells were analysed using a moving window of 6 × 6°, shifted by 2° at each step, as shown in Fig. 1c,d.

Detecting the asymmetric patterns of ΔLST_{fc}

Bubble matrix plots were used to show asymmetric responses of ΔLST_{fc} with respect to f_{gain} versus f_{loss}. As shown in Supplementary Fig. 28, in the bubble matrix, the colour of each cell represents the average value of ΔLST_{fc} observed for a given combination of f_{gain} and f_{loss} within the 0.05° grid cell. Red denotes a warming effect ($\Delta LST_{fc} > 0.02$ °C), blue indicates cooling ($\Delta LST_{fc} < -0.02$ °C) and grey represents a net-zero temperature change ($\Delta LST_{fc} = 0.0 \pm 0.02$ °C) between 2000 and 2012. The x and y axes representing the f_{loss} and f_{gain}, respectively, were plotted schematically in the 0.2 bin in Supplementary Fig. 28 and the 0.02 bin in Fig. 2.

The LST-neutral curve was defined as the boundary between dots with negative ΔLST_{fc} (cooling) and dots with positive ΔLST_{fc} (warming) in the (f_{gain}, f_{loss}) space. To simulate the LST-neutral curve, we selected the dots with $\Delta LST_{fc} = 0 \pm 0.02$ °C in the bubble matrix plots (Fig. 2). We then examined multiple linear and nonlinear (for example, quadratic, cubic and general additive models) regressions to fit the relationships between f_{gain} and f_{loss} and used the Akaike information criterion to select the optimal model[91]. Finally, a quadratic function was chosen as the best model to regress the nonlinear relationship between f_{gain} and f_{loss} where $\Delta LST_{fc} = 0 \pm 0.02$ °C: $f_{gain} = q(f_{loss})$, as depicted by the black solid curves in Fig. 2.

Assessing changes in surface energy balance

Net solar radiation received on the ground is converted into sensible heat flux (H), latent heat flux (LE) and ground heat flux (G). The function of the surface energy balance is expressed as follows[13]:

$$\mathrm{SW}_{\downarrow} - \mathrm{SW}_{\uparrow} + \mathrm{LW}_{\downarrow} - \mathrm{LW}_{\uparrow} = \mathrm{LE} + H + G \quad (6)$$

where $\mathrm{SW}_{\downarrow}$ and $\mathrm{SW}_{\uparrow}$ denote the downwelling shortwave radiative flux incidenting on the ground (total solar radiation) and reflected solar shortwave radiation from the surface (reflected shortwave radiation), respectively. Values $\mathrm{LW}_{\downarrow}$ and $\mathrm{LW}_{\uparrow}$ denote the longwave radiation from the atmosphere (atmospheric downward radiation) and longwave radiation emitted from the surface to the atmosphere (surface emitted radiation), respectively. LE is the latent heat flux referring to the transfer of heat due to the transitional phase of water in the atmosphere. Variable H is the sensible heat flux referring to the heat transfer between the ground and air caused by the turbulent movement of the surface layer. Variable G is the ground heat flux representing the quantity of energy transfer between the surface and deep soil.

Herein, we used the method of ref. 13 to assess the potential impact of tree cover changes on the surface energy balance, which assumed that the tree cover change at 30 m resolution is not strong enough to induce cloud feedback and the assigned net-zero change in $\mathrm{SW}_{\downarrow}$ and $\mathrm{LW}_{\downarrow}$ ($\Delta\mathrm{SW}_{\downarrow} = 0$ and $\Delta\mathrm{LW}_{\downarrow} = 0$) (ref. 92). The change in residual fluxes, composed of both H and G, can be estimated by equation (7). Steps for the derivation of equation (7) are shown in the Supplementary Methods.

$$\Delta(H+G)_{\mathrm{fc}} = -\Delta\mathrm{SW}_{\uparrow,\mathrm{fc}} - \Delta\mathrm{LW}_{\uparrow,\mathrm{fc}} - \Delta\mathrm{LE}_{\mathrm{fc}} \quad (7)$$

where Δ refers to the changes in the components of the surface energy balance; the subscript fc represents changes in energy fluxes induced by tree cover changes; $\Delta\mathrm{LE}_{fc}$ was calculated by removing the average ΔLE of reference undisturbed grid cells from that of corresponding disturbed forest grid cells.

The changes in the reflected shortwave radiation ($\Delta\mathrm{SW}_{\uparrow,\mathrm{fc}}$) in response to tree cover changes can be expressed as the product of changes in albedo (Δalbedo) and shortwave downwelling radiative fluxes ($\mathrm{SW}_{\downarrow}$), shown in equation (8).

$$\Delta\mathrm{SW}_{\uparrow,\mathrm{fc}} = \Delta\mathrm{albedo} \times \mathrm{SW}_{\downarrow} \quad (8)$$

The changes in $\mathrm{LW}_{\uparrow,\mathrm{fc}}$ (referred to as $\Delta\mathrm{LW}_{\uparrow,\mathrm{fc}}$) in response to tree cover change can be physically derived using equation (9) (ref. 23):

$$\Delta\mathrm{LW}_{\uparrow,\mathrm{fc}} = \epsilon \Delta\mathrm{LST}_{\mathrm{fc}} 4\sigma \mathrm{LST}^3 \quad (9)$$

where ε is broadband emissivity and σ represents the Stefan–Boltzmann constant ($\sigma = 5.67 \times 10^{-8}$ W (m^{-2} K^{-4})). MOD11C3 products[38] provide emissivity estimates, where ε can be calculated using an empirical equation[93]: $\epsilon = 0.2122\epsilon_{29} + 0.3859\epsilon_{31} + 0.4029\epsilon_{32}$. Values ϵ_{29}, ϵ_{31} and ϵ_{32} represent the estimated emissivity in MODIS bands 29 (8,400–8,700 nm), 31 (10,780–11,280 nm) and 32 (11,770–12,270 nm).

The data sources of the components in surface energy balance are shown in Supplementary Table 1. The LE data for calculating ΔLE were derived from the MOD16A3GF v.061 products[58]. The albedo and $\mathrm{SW}_{\downarrow}$ data for calculating $\Delta\mathrm{SW}_{\uparrow,\mathrm{fc}}$ were obtained from MCD43C3 v.061 products at a 0.05° resolution and from GLASS DSR (v.60) data at a 0.05° resolution[59], respectively. The daytime and night time LST data were derived from the MOD11C3 v.061 LST products[38], while the daily mean ΔLST_{fc} for estimating $\Delta\mathrm{LW}_{\uparrow,\mathrm{fc}}$ was calculated as the average of the daytime and night time ΔLST_{fc}. The $\Delta(H+G)_{fc}$ component was calculated from $\Delta\mathrm{SW}_{\uparrow,\mathrm{fc}}$, $\Delta\mathrm{LW}_{\uparrow,\mathrm{fc}}$ and $\Delta\mathrm{LE}_{fc}$ based on equation (7).

Uncertainty analysis

To assess potential uncertainties caused by scale transformation[94] that might be induced by matching 30 m resolution tree cover changes[15] with the 0.05° resolution MODIS land cover and LST data[39], we produced additional bubble matrix plots of ΔLST_{fc} at 0.1° resolution (Supplementary Fig. 6) to compare with those at 0.05° resolution (Fig. 2). If the LST-neutral curves at the 0.1° and 0.05° resolutions varied significantly ($P < 0.001$), the asymmetric patterns of ΔLST_{fc} were treated as strongly scale-dependent transformation or otherwise were considered scale-independent or rarely scale-dependent. To assess potential uncertainties from our assumptions on f_{gain} in GFW tree cover data, we additionally plotted the asymmetric patterns of ΔLST_{fc} against f_{gain} versus f_{loss} under different scenarios for pixels with tree cover gain, whose final tree covers in 2012 were assumed to be 50% (minimum), 75% (moderate) and 100% (maximum), respectively (Supplementary Figs. 3–5).

On GFW maps, the pixels of tree cover loss were recorded separately in each year from 2000 to 2012, while the pixels of tree cover gain were only given for the whole period without planting year information[15]. To allocate the fractions of tree cover gains to each year from 2000 to 2012, we overlaid the GFW tree cover change map onto a 30 m resolution global dataset of tree plantations[50]. We subsequently assigned the information on planting years to corresponding 30 m resolution pixels labelled as tree cover gain on GFW maps. Considering the inconsistency in coverage between GFW tree cover maps and the tree plantation maps[50], only the 0.05° resolution grid cells, with >80% of total 30 m resolution pixels being assigned with planting year information, were included in the analysis. After allocating the fractions of tree cover gain yearly, we examined the asymmetric responses of ΔLST_{fc} and corresponding neutral curves for various combinations of f_{gain} and f_{loss} in the different time periods (2003–2012, 2006–2012 and 2009–2012) (Supplementary Fig. 2).

Next, by matching tree age information[50] with GFW tree cover maps, we quantified the influences of tree age on the asymmetric patterns of ΔLST_{fc} and corresponding LST-neutral curves for pixels at 0.05° resolution with different tree planting ages (ages ≤6 years versus 6 years < ages ≤12 years) (Supplementary Figs. 15 and 16). Additionally, we further used the space-for-time method over a longer period to quantify the impact of tree age on ΔLST_{fc} (Fig. 5). By matching the global tree plantation data of ref. 50 with the MODIS LST time-series, we estimated the ΔLST_{fc} by using the LST of forest grid cells minus the LST of reference non-forest grid cells within a 50 km radius of the forest grid cell[5]. Only the 0.05° resolution forest grid cells with >80% of their subgrid 30 m resolution forest pixels assigned with information of planting trees based on the ref. 50 map were included in the analysis. To eliminate the influences of tree cover, forest grid cells with $50\% < f_{gain} \le 70\%$ (Supplementary Fig. 17a,c,e) and $f_{gain} > 70\%$ (Supplementary Fig. 17b,d,f)) were analysed separately.

Others[40] classified five main drivers of tree cover loss in global forests (10 km resolution): commodity-driven deforestation (permanent conversion from forestland to non-forest land), forestry (large-scale forestry operations within forests), shifting agriculture (conversion from forest to agriculture lands), wildfire (burning of forest vegetation) and urbanization (conversion from forest to urban areas). To investigate the underlying mechanism, we graphed the bubble matrix plots of ΔLST_{fc} and changes in energy fluxes against f_{gain} and f_{loss} for disturbed forest grid cells with different drivers of tree cover loss, respectively (Supplementary Figs. 9–14).

Finally, we used five regional forest cover datasets in Canada[65], the United States[66], eastern Europe[67], northern Europe[68], China[69] and the whole tropical region[70] (Supplementary Table 2) to test potential uncertainties from tree cover change data. For regional tree cover data, we classified the 30 m resolution pixels of f_{gain} and f_{loss} as follows: (1) forest pixels converted from other land cover types are recognized as type of 'forest gain'; (2) non-forest pixels converted from forests are detected as type of 'forest loss'; (3) pixels having ever undergone both processes (1) and (2) are recognized as type of 'forest gain and loss'. Then, we compared f_{gain} and f_{loss} in GFW tree cover data with those of the regional tree cover datasets, calibrated by national forest cover statistics or field forest inventory data (Supplementary Fig. 20), at 0.05° resolution and tested the asymmetric patterns of ΔLST_{fc} in response to f_{gain} versus f_{loss} (Supplementary Figs. 21–26).

Data availability

The LST, land cover, evapotranspiration, albedo, forest age and energy flux data used for the analyses in this study are available online as follows: 30 m resolution GFW maps of twenty-first century forest cover change https://glad.earthengine.app/view/global-forest-change; MOD11C3 LST product https://lpdaac.usgs.gov/products/mod11c3v061/; MCD12C1 Land Cover dataset https://lpdaac.usgs.gov/products/mcd12c1v061/; MCD43C3 Albedo product https://lpdaac.usgs.gov/products/mcd43c3v061/; MOD16A2GF ET and LE product https://lpdaac.usgs.gov/products/mod16a2v061/; GLASS Shortwave Radiation product http://www.glass.umd.edu/Download.html; MOD13C2 NDVI product https://lpdaac.usgs.gov/products/mod13c2v061/; drivers of global forest loss https://www.science.org/doi/abs/10.1126/science.aau3445; GLASS ET product http://www.glass.umd.edu/Download.html; PML_V2 ET product https://data.tpdc.ac.cn/zh-hans/data/48c16a8d-d307-4973-abab-972e9449627c/; the latest digital Köppen-Geiger world map http://koeppen-geiger.vu-wien.ac.at/present.htm; global map of planting years https://figshare.com/articles/dataset/A_global_map_of_planting_years_of_plantations/19070084/1; forest cover change data of Canada https://opendata.nfis.org/mapserver/nfis-change_eng.html; forest cover change data of northern Europe https://land.copernicus.eu/pan-european/high-resolution-layers/forests/tree-cover-density/change-maps; forest cover change data of eastern Europe https://glad.geog.umd.edu/dataset/eastern-europe-forset-cover-dynamics-1985-2012/; forest cover change data of the United States https://www.mrlc.gov/data; and forest cover change data of the whole tropical region https://forobs.jrc.ec.europa.eu/TMF/.

Code availability

The code used for this analysis is available in a Zenodo repository at https://doi.org/10.5281/zenodo.8088598 (ref. 95).

References

91. Sakamoto, Y., Ishiguro, M. & Kitagawa, G. *Akaike Information Criterion Statistics* (D. Reidel, 1986).
92. Zhang, M. et al. Response of surface air temperature to small-scale land clearing across latitudes. *Environ. Res. Lett.* **9**, 034002 (2014).
93. Wang, K. et al. Estimation of surface long wave radiation and broadband emissivity using Moderate Resolution Imaging Spectroradiometer (MODIS) land surface temperature/emissivity products. *J. Geophys. Res. Atmos.* **110**, D11109 (2005).
94. Chen, J. M. Spatial scaling of a remotely sensed surface parameter by contexture. *Remote Sens. Environ.* **69**, 30–42 (1999).
95. Zhang, C. Code to support 'Asymmetric influence of forest cover gain and loss on land surface temperature'. *Zenodo* https://doi.org/10.5281/zenodo.8088598 (2023).

Acknowledgements

We thank N. Coops from the University of British Columbia and S. Bartalev from the Russian Academy of Sciences for providing the regional tree cover datasets and editing the paper. This study was supported by the National Natural Science Foundation of China (grant nos. 41971275, 31971458 and U21A6001).

Author contributions

Y.S. and X.C. designed the study and wrote the initial manuscript. Y.S. and C.Z. collected the data and performed the analysis. P.C., Z. Zeng, A.C., J.S., J.M.C., J.L., Y.-P.W., W.Y., S.P., X. Lee, Z. Zhu and Y.L. contributed to discuss the scientific question and revise the manuscript. All authors reviewed and approved the manuscript.

Competing interests

The authors declare no competing interests.

Additional information

Supplementary information The online version contains supplementary material available at https://doi.org/10.1038/s41558-023-01757-7.

Correspondence and requests for materials should be addressed to Xiuzhi Chen.

Peer review information *Nature Climate Change* thanks David Ellison, Shani Rohatyn and the other, anonymous, reviewer(s) for their contribution to the peer review of this work.

Reprints and permissions information is available at www.nature.com/reprints.